ChemPubSoc Europe

DOI: 10.1002/chem.201503099

CHEMISTRY A European Journal Communication

Solar Cells

Facile Synthesis of a Furan–Arylamine Hole-Transporting Material for High-Efficiency, Mesoscopic Perovskite Solar Cells

Anurag Krishna,[a] Dharani Sabba,[b] Jun Yin,[d] Annalisa Bruno,[b] Pablo P. Boix,[b] Yang Gao,[c] Herlina A. Dewi,[b] Gagik G. Gurzadyan,[d] Cesare Soci,[d] Subodh G. Mhaisalkar,*[b] and Andrew C. Grimsdale*[c]

Abstract: A novel hole-transporting molecule (F101) based on a furan core has been synthesized by means of a short, high-yielding route. When used as the hole-transporting material (HTM) in mesoporous methylammonium lead halide perovskite solar cells (PSCs) it produced better device performance than the current state-of-the-art HTM 2,2′,7,7′-tetrakis-(*N*,*N*-di-*p*-methoxyphenylamine)-9,9′-spirobifluorene (spiro-OMeTAD). The F101-HTM-based device exhibited both slightly higher J_{sc} (19.63 vs. 18.41 mA cm^{-2}) and V_{oc} (1.1 vs. 1.05 V) resulting in a marginally higher power conversion efficiency (PCE) (13.1 vs. 13%). The steady-state and time-resolved photoluminescence show that F101 has significant charge extraction ability. The simple molecular structure, short synthesis route with high yield and better performance in devices makes F101 an excellent candidate for replacing the expensive spiro-OMeTAD as HTM in PSCs.

Organic–inorganic metal halide perovskites, particularly methylammonium lead iodide ($CH_3NH_3PbI_3$) have recently emerged as high performance and low cost materials for solar cell applications.[1–3] Methylammonium lead halide perovskites have large exciton diffusion lengths, high extinction coefficients, direct bandgap and excellent absorption throughout the UV/Vis/NIR spectrum.[4,5] These attributes makes these perovskites excellent material for light harvesting, and they have been used as light absorbers for mesoscopic metal oxides and planar heterojunction solar cells. In 2012 Grätzel, Park et al. reported a solid-state device using $CH_3NH_3PbI_3$ as the light absorber and 2,2′,7,7′-tetrakis-(*N*,*N*-di-*p*-methoxyphenylamine)-9,9′-spirobifluorene (spiro-OMeTAD) as a hole-transporting material (HTM), from which a very promising power conversion efficiency (PCE) of 9.7% was obtained.[2] Since that report, the development of lead halide perovskite based, solid-state devices has been remarkable with PCEs up to 20% being reported.[3,6–8] Spiro-OMeTAD is the most commonly used HTM in these devices due to its superior performance. Unfortunately the cost of spiro-OMeTAD remains very high, largely because of its multistep, low-yielding synthesis. This limitation in HTM options has proved to be a major impediment to the growth and advancement of high-efficiency, cost-effective perovskite solar cells. Hence, it is imperative to develop alternative HTMs, which have at least equal performance to spiro-OMeTAD and are more economic to make. A number of conjugated polymers including poly(3-hexylthiophene) (P3HT), and poly(triarylamine) (PTAA) have been employed as HTMs, but the results are inferior to spiro-OMeTAD.[9] A wider range of small molecules based on ethylenedioxythiophene,[10a] thiophene,[10b] cruciform oligothiophenes,[11] pyrene,[12] triptycene,[13] triazines,[14] conjugated quinolizino acridine,[15] carbazole,[16] and planar triphenylamine[17] have also been investigated. The best of these show similar or superior performance to spiro-OMeTAD in some aspects, but no material has yet emerged clearly superior to it in cost, device efficiency, and stability. Hence the challenge remains to make simple, inexpensive, high-performance HTMs.

Here we report a novel HTM, which we denote F101 and which contains an electron-rich furan core linked to triphenyl amine moieties (Figure 1a). The planar structure of the molecule and smaller size of the O atom in the ring compared to S in our previously reported thiophene-based HTMs[10a,b] should result in closer intermolecular π–π stacking, which could be beneficial for enhancing the hole transport and also increase the lifetime of charge carriers. Furthermore, the small molecular size of the HTM could lead to better pore filling of the mesoporous TiO_2 layer loaded perovskite. F101 was synthesized from a relatively inexpensive commercially available furan derivative in a single step with high yield and has high solubility in common organic solvents. Mesoscopic perovskite solar cells

[a] *A. Krishna*[+]
Energy Research Institute, Interdisciplinary Graduate School Nanyang Technological University (Singapore)

[b] *Dr. D. Sabba,*[+] *Dr. A. Bruno, Dr. P. P. Boix, Dr. H. A. Dewi, Prof. S. G. Mhaisalkar*
Energy Research Institute @ NTU (ERI@N)
Nanyang Technological University, 50 Nanyang Drive
Singapore 637553 (Singapore)
E-mail: Subodh@ntu.edu.sg

[c] *Y. Gao, Prof. A. C. Grimsdale*
School of Materials Science and Engineering
Nanyang Technological University, Nanyang Avenue
Singapore 637553 (Singapore)
E-mail: acgrimsdale@ntu.edu.sg

[d] *J. Yin, Dr. G. G. Gurzadyan, Prof. C. Soci*
Division of Physics and Applied Physics
Nanyang Technological University, 21 Nanyang Link
Singapore 637371 (Singapore)

[+] *Authors contributed equally.*

Supporting information and ORCID(s) from the author(s) for this article is available on the WWW under http://dx.doi.org/10.1002/chem.201503099.

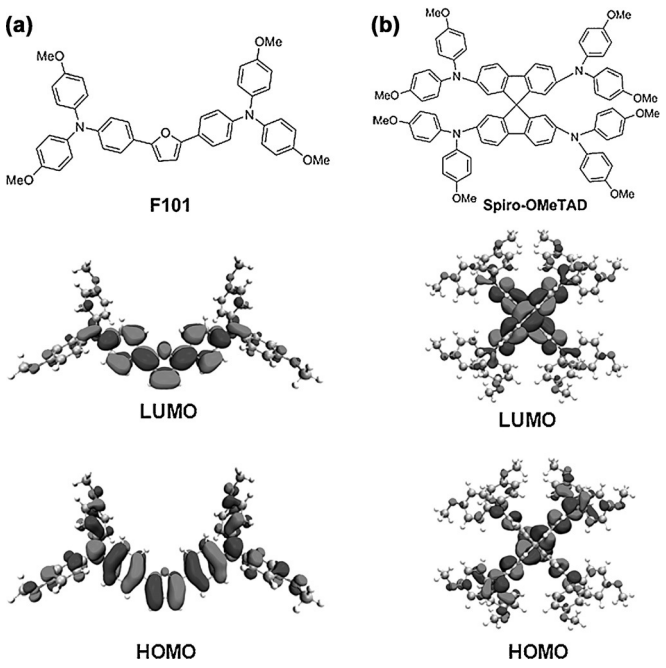

Figure 1. a) Chemical structure of F101, electronic density distribution of lowest unoccupied molecular orbital (LUMO) and highest occupied molecular orbital (HOMO) for F101; b) chemical structure of spiro-OMeTAD, electronic density distribution of LUMO and HOMO for spiro-OMeTAD.

fabricated using F101 outperformed the state-of-the-art HTM spiro-OMeTAD, showing efficiencies over 13% with a remarkably high open circuit voltage of 1.1 V. To the best of our knowledge, this is the first reported furan-based small molecule HTM for perovskite solar cells (PSCs).

In the molecular design HTMs, the heteroatom (such as Group 16 atoms) is used in the building block to adjust HOMO and LUMO levels, while the hole-accepting ability of the material is produced by the N atoms of diphenylamine.[18] In a previous study it has been demonstrated that the interaction between terminal methoxybenzene groups ($CH_3OC_6H_5$) of spiro-OMeTAD and $CH_3NH_3PbI_3$ is important for efficient hole transfer, especially on the preferred (001) and (110) surfaces.[19] So F101 has four anchored terminal methoxybenzene groups for enhanced hole transport. From the electron density distribution diagrams, it is observed that the electronic cloud of F101 delocalizes over the whole molecule in the HOMO (Figure 1a), while for the LUMO, it is mainly localized on the central furan and benzene units (Figure 1a). Thus, the planar central units of F101 play a dual role in PSCs: 1) they enhance the electronic cloud overlapping between HOMO of F101 and valence band maximum of $CH_3NH_3PbI_3$, and 2) they improve the hole transporting mobility due to large electronic coupling between F101 molecules at short intermolecular distances. The HOMO level (−4.23 eV) of F101 calculated by density functional theory (DFT, see Supporting Information) is slightly higher than that of spiro-OMeTAD (−4.48 eV), which could facilitate better hole transfer between F101 and perovskite.

In conjunction with its predicted material properties, the short efficient synthesis route of F101 makes it an attractive HTM for perovskite solar cell industry. The synthesis route of F101 is very much shorter and less expensive as compared to spiro-OMeTAD (Scheme 1). The commercially available relatively inexpensive 2,5-dibromofuran was Suzuki coupled with triphenylamine boronic acid derivative to give F101 in 65% yield as shown in Scheme 1. The molecular structure was confirmed by ^1H and ^{13}C NMR spectroscopy and MALDI-TOF mass spectrometry (see the Supporting Information).

The opto-electronic properties of F101 have been investigated and compared to those of spiro-OMeTAD. In the UV/Vis absorption spectra (shown in Figure 2a), F101 and spiro-OMeTAD showed absorption peaks centered at 393 and 385 nm respectively, that is, the absorption maxima of F101 is slightly red shifted compared to spiro-OMeTAD suggesting better conjugation in F101 than in spiro-OMeTAD. It is observed that the absorption onset wavelengths of F101 and spiro-OMeTAD are 446 and 425 nm, respectively, which corresponds to a band bap of 2.78 and 2.92 eV, respectively. Cyclic voltammograms of F101 and spiro-OMeTAD are shown in Figure 2b.Two of the redox peaks observed for F101 are highly reversible, showing that it has excellent electrochemical stability. The, HOMO energy level was calculated from the CV data using the following equation: $E_{HOMO} = -5.1-(E_{ox,HTM}$ vs. Fc/Fc+) [eV], in which $E_{ox,HTM}$ vs. Fc/Fc+ is the onset of oxidation potential of ferrocene, which is used as reference and −5.1 eV is the redox po-

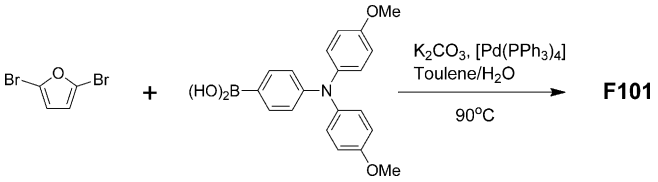

Scheme 1. Synthetic route for F101.

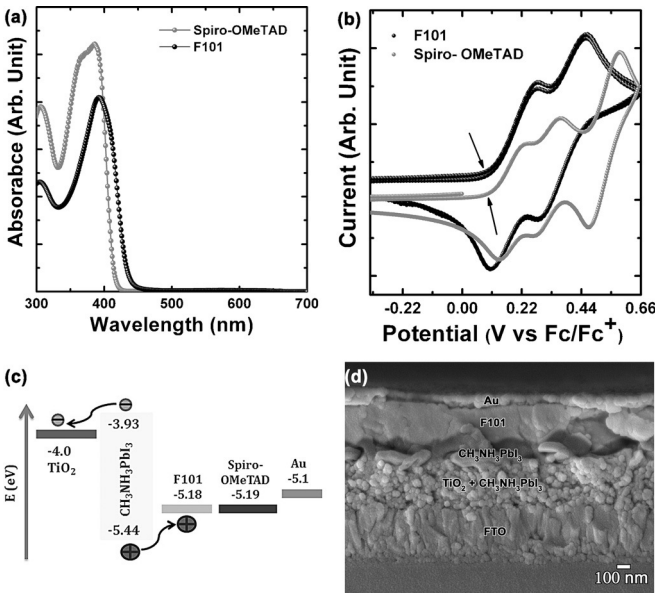

Figure 2. a) Absorption spectra for spiro-OMeTAD and F101, b) cyclic voltammogram for spiro-OMeTAD and F101, c) band diagram for the device with new HTM F101 and spiro-OMeTAD, and d) cross-sectional SEM image of device fabricated with F101.

tential of ferrocene.[20] The HOMO levels of F101 and spiro-OMeTAD as calculated from CV are −5.18 and −5.19 eV, respectively. For $CH_3NH_3PbI_3$ the reported HOMO energy level is −5.44 eV,[2] which indicates that our new HTM F101 has favorable energetics for the hole transfer (Figure 2c). The hole mobility of F101 was evaluated and compared with spiro-OMeTAD (Tables S1 and S2 in the Supporting Information) based on different transfer pathways in the predicted crystal structures (Figure S1 and S2, Supporting Information). Although the calculated hole reorganization energy of F101 (227 meV) is larger than that of spiro-OMeTAD (148 meV), the resulting hole mobilities for F101 in the three possible crystals shown in Figure S1 (2.61, 0.044, and 0.055 $cm^2V^{-1}s^{-1}$) are one order of magnitude higher than for spiro-OMeTAD (0.0065, 0.0063, and 0.0845 $cm^2V^{-1}s^{-1}$) due to large electronic coupling in the F101 crystals, especially for the face-to-face dimer configuration (pathway 4 of the *C*2/C space group shown in Figure S1) with effective π-orbital overlap, showing that F101 is a promising HTM with relatively high hole mobility. The energetics of the system employing the F101/spiro-OMeTAD are represented in Figure 2c. Table 1 summarizes the optical and electrochemical

Table 1. Optical and electrochemical properties of F101 and spiro-OMeTAD.

HTM	λ_{max} [nm]	λ_{onset} [nm]	E_g [eV][a]	E_{HOMO} [eV]	E_{LUMO} [eV][b]
F101	393	446	2.78	−5.18	−2.4
spiro-OMeTAD	385	425	2.92	−5.19	−2.27

[a] Optical band gap (E_g) obtained from the onset value of absorption (λ_{onset}). [b] LUMO calculated by LUMO = HOMO + E_g.

properties of the HTMs. The cross-sectional scanning electron microscopy (SEM) image shown in the Figure 2d show the formation of a well-defined hybrid structure with clear interfaces. The thicknesses of the TiO_2 loaded with perovskite, perovskite over layer and the HTM layer are about 300, 190 and 270 nm, respectively.

The current-density–voltage (*J*–*V*) characteristics of the devices employing F101 and spiro-OMeTAD as HTMs, together with a device without HTM are shown in Figure 3a and summarized in Table 2. The PCEs of the best performing device with F101 and spiro-OMeTAD as HTM were 13.1, and 13.0%, respectively. The best performing device fabricated without HTM had a PCE of only 5.2%, which confirms that an HTM is a vital component of high efficiency perovskite solar cells. The short circuit current densities (J_{sc}) of the cells fabricated using F101 and spiro-OMeTAD are 19.63 and 18.41 mA cm^{-2}, respectively and these are in close agreement with the J_{sc} integrated from IPCE Spectra (see supporting info Figure S6 in the Supporting Information). Also the devices with F101 showed slightly higher open circuit voltage (V_{oc} = 1.10 V) than devices employing spiro-OMeTAD (V_{oc} = 1.05 V). The V_{oc} depends on 1) the splitting of the Fermi levels for photogenerated charges, 2) the recombination, and 3) the energetics of the devices.[12,13] Since the HOMO energy levels of F101 and spiro-OMeTAD determined by CV are rather similar, the V_{oc} enhancement in case of F101-HTM-based devices could be related to the charge recombination process. Consequently, in order to compare the process of recombination, electrochemical impedance spectroscopy was carried out. The fitting of the impedance results (R_{rec} vs. applied voltage as shown in Figure 3b) followed previous models employed in perovskite solar cells, in which the resistance of the lower frequency feature is directly related to the recombination process.[21–23] In Figure 3b, it is evident that F101-based devices exhibited slightly higher recombination resistance in comparison to spiro-OMeTAD, which may be attributed to efficient charge extraction ability of F101. However the high device performance of F101 is limited by the poor fill factor (FF = 60.8%), which is attributed to a high series resistance of the device as calculated from *J*–*V* curve. In contrast, the spiro-OMeTAD-based devices exhibited better FF (67.2%). This shortcoming in F101 devices could potentially be improved by further optimization of various device components.[24,25] If the FF could be improved to match that of spiro-OMeTAD the efficiency could be improved by about 1.3%.

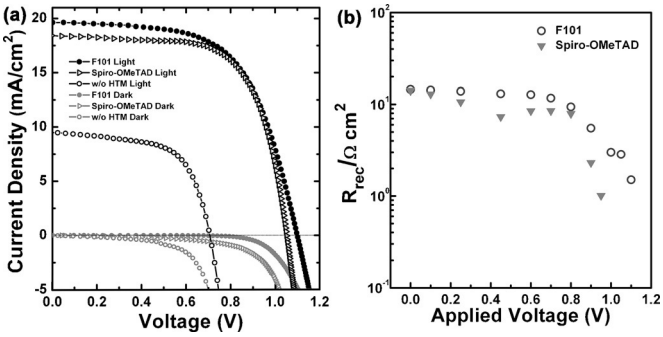

Figure 3. a) Current density vs. voltage curve under AM 1.5G illumination (100 mW cm^{-2}); b) Recombination resistance extracted from fitting of the EIS results under illumination for perovskite solar cells with F101 and spiro-OMeTAD as the HTM.

Table 2. Summary of device parameters; open circuit voltage (V_{oc}), current density (J_{sc}), fill factor (FF) and power conversion efficiency (PCE). Area = 0.2 cm^2.

HTM	J_{sc} [(mA cm^{-2}]	V_{oc} [V]	FF [%]	PCE_{max} [%]	[a]PCE_{avg} [%]
F101	19.63	1.10	60.8	13.1	13.0
spiro-OMeTAD	18.41	1.05	67.2	13.0	12.4
W/O HTM	9.58	0.70	77.5	5.2	4.9

[a] Average PCE is based on ten cells in a single batch.

To further look in to the charge-carrier dynamics at the perovskite/HTM interface, we measured steady-state and time-resolved photoluminescence (PL), whereby quenching of steady-state PL and reduction of PL lifetime are indicators of efficient charge extraction at the perovskite/HTM interface. From the PL spectra in Figure 4a, it is evident that both HTMs significantly quench perovskite emission signal, with HTM F101 having a slightly better PL quenching efficiency (ca. 97%) relative to spiro-OMeTAD (ca. 93%). Time-resolved PL measurements were

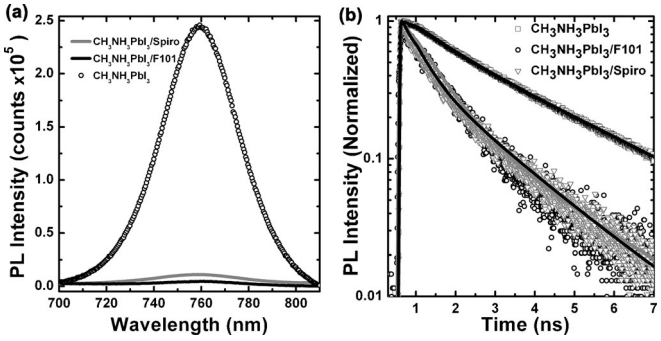

Figure 4. a) The steady-state photoluminescence (PL) spectra and b) time-resolved PL spectra of $CH_3NH_3PbI_3$, $CH_3NH_3PbI_3$/spiro-OMeTAD and $CH_3NH_3PbI_3$/F101.

carried out with excitation at 400 nm and monitoring the emission peak at 760 nm (Figure 4b). The pristine perovskite ($CH_3NH_3PbI_3$) exhibited a radiative life time of about 2.6 ns, whereas this was shorter in bilayered samples ($CH_3NH_3PbI_3$/HTM). Both HTMs spiro-OMeTAD and F101 showed similar decay time of about 1 ns. This indicates that charge pairs generated upon illumination in the perovskite are efficiently separated at the interface and then transferred to the HTM. Overall the PL data indicates that F101 and spiro-OMeTAD have comparable hole extraction ability.

In summary, we have designed and synthesized a novel HTM F101 based on a furan core, which performs at least as well as the state of the art HTM spiro-OMeTAD, while having a simpler and more economical synthesis. Its good charge injection properties enable high current densities (19.63 mA cm^{-2}), and better charge recombination resistance assists in attainment of high V_{oc} (1.1 V), yielding $>13\%$ efficiencies, comparable to spiro-OMeTAD devices. We are confident that with further optimization and fine tuning of various device parameters and by developing better understanding of interfacial characteristics, even further enhancement of device performance could be achieved. The simple synthesis with high yield and high device performance means F101 has great potential to replace the expensive and more complicated spiro-OMeTAD as an HTM in PSCs.

Experimental Section

Synthesis of 4,4′-(furan-2,5-diyl)bis(*N*,*N*-bis(4-methoxyphenyl)-aniline) (F101): 2,5-Dibromofuran (0.25 g, 1.12 mmol), {4-[bis(4-methoxyphenyl)amino]phenyl}boronic acid[26] (0.825 g, 2.35 mmol), [$Pd^0(PPh_3)_4$] (0.13 g, 0.1 mmol), K_2CO_3 (5 mL, 2 M) and degassed toluene (20 mL) were transferred in to a 50 mL round-bottomed flask. The reaction mixture was then stirred at 95 °C under nitrogen for 48 h and then was cooled down to room temperature, poured into water, extracted with CH_2Cl_2 and washed with water. The organic layer was dried over $MgSO_4$ and concentrated, and the residue mixture was purified by column chromatography on silica gel eluting with CH_2Cl_2/hexane 3:2 (v/v) to obtain the product as a yellow solid (0.48 g, 65%). ^{1}H NMR ([D$_6$]DMSO, 400 MHz): $\delta = 7.594$ (d, $J =$ 8.8 Hz, 4H), 7.082 (d, $J = 8.8$, 8H), 6.968 (d, $J = 8.8$ Hz, 8H), 6.851 (d, $J = 8.8$ Hz, 4H), 6.811 (S, 2H), 3.781 ppm (s, 12H); ^{13}C NMR ([D$_6$]DMSO, 100 MHz): $\delta = 156.72$, 153.08, 148.44, 140.79, 127.55, 125.21, 123.31, 120.40, 115.89, 107.04, 56.15 ppm; HRMS (MALDI-TOF): *m/z* calcd for $C_{44}H_{38}N_2O_5$, 674.80; found: 674.05.

Device fabrication: Fluorine-doped tin oxide (FTO, $<14\ \Omega$ per square, 2.2 mm thick) substrates were laser etched to form the desired pattern, which were subsequently cleaned by sonication in decon soap solution, followed by ethanol. A thin compact layer of TiO_2, which acted as a blocking layer between FTO and perovskite and was about 80–100 nm, was deposited by aerosol spray-pyrolysis, using titanium diisopropoxide bis(acetylacetonate) (75 wt.% in isopropanol) and absolute ethanol in the ratio 1:9 by volume and ambient air was used as the carrier gas. Then these substrates were annealed at 450 °C for 30 min and then were treated with 100 mM of $TiCl_4$ solution for 60 min at 70 °C, followed by rinsing with deionized water and ethanol and subsequent annealing at 500 °C for 1 h. The mesoporous TiO_2 layer composed of 30 nm-sized particles was deposited by spin coating at 4000 r.p.m. for 30 s using a commercial TiO_2 paste (Dyesol DSL 30 NRD) diluted in ethanol (2:7, weight ratio). After drying at 125 °C, the TiO_2 films were gradually heated to 500 °C, baked at this temperature for 15 min, and cooled to room temperature. An organic–inorganic perovskite (CH_3NH_3)PbI_3 was deposited by a sequential method[3] under a controlled environment. Lead iodide (1 M) was dissolved in *N*,*N*-dimethylformamide (DMF) overnight under stirring conditions at 70 °C and was spincoated onto the substrates at 6000 r.p.m for 5 s. These substrates were then dried for 30 mins at 70 °C. Subsequently the films were dipped in 8 mg mL^{-1} solution of CH_3NH_3I in 2-propanol for 20 min, were rinsed with 2-propanol, and were spincoated at 4000 rpm for 30 s. After drying, the films were annealed at 100 °C for 30 min. The HTMs F101 and spiro-OMeTAD were dissolved in chlorobenzene (90 and 100 mg mL^{-1}, respectively) and spincoated on these substrates. Additives like Li(CF_3SO_2)$_2$N, *tert*-butylpyridine and tris[2-(1*H*-pyrazol-1-yl)pyridine]cobalt(III) (FK102) dopant were added to the above solution as stated in literature.[3] The masked substrates were placed in a thermal evaporator for gold (Au) deposition by shadow masking. The thickness of the Au electrode was about 100 nm and an active area of 0.2 cm^2 was defined by the overlap of TiO_2 and Au.

Acknowledgements

This work was funded by National Research Foundation (NRF) Singapore (CRP Award no.: NRF-CRP4-2008-03 and NRF2014NRF-CRP002-036), Singapore Ministry of Education (MOE2013-T2-044) and the Singapore–Berkeley Research Initiative for Sustainable Energy (SinBeRISE) CREATE Programme. We would like to thank Wee Choon Lock for his help in the synthesis.

Keywords: heterocycles · hole transport · perovskite · solar cells

[1] M. M. Lee, J. Teuscher, T. Miyasaka, T. N. Murakami, H. J. Snaith, *Science* **2012**, *338*, 643–647.
[2] H. Kim, J. H. Im, C. R. Lee, K. B. Lee, T. Moehl, A. Marchioro, S. J. Moon, R. H. Baker, J. H. Yum, J. E. Moser, M. Grätzel, N. G. Park, *Sci. Rep.* **2012**, *2*, 591.
[3] J. Burschka, N. Pellet, S. J. Moon, R. Humphry-Baker, P. Gao, M. K. Nazeeruddin, M. Grätzel, *Nature* **2013**, *499*, 316–319.
[4] T. Salim, S. Sun, Y. Abe, A. Krishna, A. C. Grimsdale, Y.-M. Lam, *J. Mater. Chem. A* **2014**, *2*, 10532.

[5] A. Kojima, K. Teshima, Y. Shirai, T. Miyasaka, *J. Am. Chem. Soc.* **2009**, *131*, 6050 – 6051.
[6] M. Liu, M. B. Johnston, H. J. Snaith, *Nature* **2013**, *501*, 395 – 398.
[7] H. Zhou, Q. Chen, G. Li, S. Luo, T.-B. Song, H.-S. Duan, Z. Hong, J. You, Y. Liu, Y. Yang, *Science* **2014**, *345*, 542 – 546.
[8] N. J. Jeon, J. H. Noh, Y. C. Kim, W. S. Yang, S. Ryu, S. I. Seok, *Nat. Mater.* **2014**, *13*, 897 – 903.
[9] J. H. Heo, S. H. Im, J. H. Noh, T. N. Mandal, C. S. Lim, J. Chang, Y. H. Lee, H. J. Kim, A. Sarkar, M. K. Nazeeruddin, M. Grätzel, S. Seok, *Nat. Photonics* **2013**, *7*, 486 – 491.
[10] a) H. Li, K. Fu, A. Hagfeldt, M. Grätzel, S. G. Mhaisalkar, A. C. Grimsdale, *Angew. Chem. Int. Ed.* **2014**, *53*, 4085 – 4088; *Angew. Chem.* **2014**, *126*, 4169 – 4172; b) H. Li, K. Fu, P. P. Boix, L. H. Wong, A. Hagfeldt, M. Grätzel, S. G. Mhaisalkar, A. C. Grimsdale, *ChemSusChem* **2014**, *7*, 3420 – 3425.
[11] T. Krishnamoorthy, K. Fu, P. P. Boix, H. Li, T. M. Koh, W. L. Leong, S. Powar, A. C. Grimsdale, M. Grätzel, N. Mathews, S. G. Mhaisalkar, *J. Mater. Chem. A* **2014**, *2*, 6305 – 6309.
[12] N. J. Jeon, J. Lee, J. H. Noh, M. H. Nazeeruddin, M. Grätzel, S. I. Seok, *J. Am. Chem. Soc.* **2013**, *135*, 19087 – 19090.
[13] A. Krishna, D. Sabba, H. Li, J. Yin, P. P. Boix, C. Soci, S. G. Mhaisalkar, A. C. Grimsdale, *Chem. Sci.* **2014**, *5*, 2702 – 2709.
[14] K. Do, H. Choi, K. Lim, H. Jo, J. W. Cho, M. K. Nazeeruddin, J. Ko, *Chem. Commun.* **2014**, *50*, 10971 – 10974.
[15] P. Qin, S. Paek, M. I. Dar, N. Pellet, J. Ko, M. Grätzel, M. K. Nazeeruddin, *J. Am. Chem. Soc.* **2014**, *136*, 8516 – 8519.
[16] B. Xu, E. Sheibani, P. Liu, J. Zhang, H. Tian, N. Vlachopoulos, G. Boschloo, L. Kloo, A. Hagfeldt, L. Sun, *Adv. Mater.* **2014**, *26*, 6629 – 6634.
[17] H. Choi, S. Paek, N. Lim, Y. H. Lee, M. K. Nazeeruddin, J. Ko, *Chem. Eur. J.* **2014**, *20*, 10894 – 10899.
[18] J. Yin, S. L. Zhang, R. F. Chen, Q. D. Ling, W. Huang, *Phys. Chem. Chem. Phys.* **2010**, *12*, 15448 – 15458.
[19] J. Yin, D. Cortecchia, A. Krishna, S. Chen, N, Mathews, A. C. Grimsdale, C. Soci, *J. Phys. Chem. Lett.* **2015**, *6*, 1396 – 1402.
[20] C. M. Cardona, W. Li, A. E. Kaifer, D. Stockdale, G. C. Bazan, *Adv. Mater.* **2011**, *23*, 2367 – 2371.
[21] A. Dualeh, T. Moehl, N. Tetreault, J. Teuscher, P. Gao, M. K. Nazeeruddin, M. Grätzel, *ACS Nano* **2014**, *8*, 362 – 373.
[22] V. Gonzalez-Pedro, E. J. Juarez-Perez, W. S. Arsyad, E. M. Barea, F. Fabregat-Santiago, I. Mora-Sero, J. Bisquert, *Nano Lett.* **2014**, *14*, 888 – 893.
[23] H. S. Kim, J. W. Lee, N. Yantara, P. P. Boix, S. A. Kulkarni, S. G. Mhaisalkar, M. Grätzel, N.-G. Park, *Nano Lett.* **2013**, *13*, 2412 – 2417.
[24] N. Marinova, W. Tress, R. Humphry-Baker, M. I. Dar, V. Bojinov, S. M. Zakeeruddin, M. K. Nazeerddin, M. Grätzel, *ACS Nano* **2015**, *9*, 4200 – 4209.
[25] Q. Wang, C. Bi, J. Huang, *Nano Energy* **2015**, *15*, 275 – 280.
[26] C. Teng, X. Yang, C. Yang, S. Li, M. Cheng, A. Hagfeldt, L. Sun, *J. Phys. Chem. C* **2010**, *114*, 9101 – 9110.

Received: August 6, 2015
Published online on September 3, 2015